

Phenotype characterization of pericytes during tissue repair following low-level laser therapy

Alena Medrado¹, Tila Costa², Thiago Prado¹, Sílvia Reis³ & Zilton Andrade¹

¹Laboratory of Experimental Pathology, Oswaldo Cruz Foundation, Salvador, Brazil, ²Basic Science Department, Foundation for the Development of Science, Salvador, Brazil, and ³Diagnostics and Therapeutics Department, Federal University of Bahia, Salvador, Brazil

Summary

Key words:

extracellular matrix; photobiostimulation; wound repair

Correspondence:

Alena Peixoto Medrado, Laboratory of Experimental Pathology, Oswaldo Cruz Foundation, Salvador, Brazil.
e-mail: alenamedrado@hotmail.com

Accepted for publication

14 April 2010

Conflicts of interest:

None declared.

Background/purpose: The action of low-level laser therapy (LLLT) on pericytes during wound healing is not well established. The objective of this study was to identify the effect of laser treatment on pericytes during tissue repair.

Methods: Punch biopsies were performed on 40 Wistar rats. Twenty animals had their wounds treated with a dose of 4 J/cm² using a 670 nm diode laser (9 mW output, 0.031 W/cm²) every other day, while the controls received sham irradiation. Animals were sacrificed 3, 7, 10 and 14 days after punch biopsy. Immunohistochemistry staining with anti-desmin, anti-smooth muscle α -actin and anti-NG2 antibodies was used to characterize and count pericytes around blood vessels and myofibroblasts dispersed in the extracellular matrix (ECM). The morphology of pericytes was confirmed by transmission electronic microscopy.

Results: The laser group exhibited significantly more smooth muscle α -actin-positive staining cells at day 7 and more desmin-positive staining cells at day 10 around blood vessels. Laser treatment was also associated with higher numbers of NG2-positive staining cells, especially on days 3 and 7 post-biopsy ($P < 0.05$). Ultrastructural findings confirmed the presence of pericytes sharing the basal membrane with endothelial cells.

Conclusion: LLLT stimulated the proliferation and migration of pericytes to the ECM and their phenotypic modulation to myofibroblasts.

During the last 30 years, low-level laser therapy (LLLT) has been studied by many scientific groups. A great deal of information about its effects on cellular mechanisms has been established. LLLT is able to alter cellular metabolism, especially by interfering with the mitochondrial-membrane potential and ATP synthesis (1, 2). Furthermore, it stimulates the cell cycle and increases cellular proliferation (3–5). Through biostimulation, LLLT can accelerate wound healing by improving blood flow, vasodilatation and angiogenesis (6, 7).

Little is known about the interaction between LLLT and pericytes. Pericytes originate from the mesenchymal lineage of smooth muscle cells and share the basal membrane of blood vessels with endothelial cells (8). They often proliferate during wound healing, especially with the formation of granulation tissue, which is a source of angiogenesis and fibroblast proliferation (9). Pericytes form long cytoplasmic projections that encircle the endothelial tube, making specialized junctions and focal contacts with endothelium (10). Additionally, these cells influence blood vessel stability through extracellular matrix (ECM) deposition and activation or production of molecules that promote endothelial cells differentiation or quiescence (11).

Pericytes may also differentiate into osteoblasts, chondrocytes, fibroblasts, adipocytes and smooth muscle cells (12). Although there are no specific antibodies for pericytes, they may be identified in granulation tissue by immunohistochemical staining for smooth muscle α -actin (SM- α actin), desmin and NG2. Particularly, NG2 (chondroitin sulfate proteoglycan) has been described in cardiomyocytes, in developing microvasculature by smooth muscle cells, and in nascent microvessels by vascular pericytes (13). However, besides immunohistochemistry, ultrastructural features are decisive for pericytes identification (8, 14).

The present study was aimed at investigating the effects of 670 nm LLLT on pericytes and their role in tissue repair using a rat model of wound healing.

Materials and methods

All animal experiments were carried out in compliance with the laws and guidelines for experimental use and care of animals in accordance with the Committee for Ethics in Animal Experimentation, Oswaldo Cruz Foundation, Salvador, Bahia,

Brazil. The animals also received humane care in compliance with the Ethical Principles of Animal Experimentation.

Experimental groups

Forty male Wistar rats, weighing 150–250 g, kept in individual cages with good conditions of light and room temperature (26 °C), with free access to water and balanced commercial diet were used. All the animals had their dorsal skin shaved and cleaned. Under strict conditions of asepsis and anesthesia with ketamin and xylasin at a single dose of 0.2 ml per 100 g of body weight, a circle representing a portion of the skin was removed using an 8-mm-diameter circular device (Biopsy Punch, Stiefel, Germany), leaving a well-delimited and uniform skin ulcer in the center of the shaved area, which was investigated thereafter.

The animals were divided into two experimental groups.

Group I – Control: Animals with skin ulcers were subjected to sham irradiations. With the apparatus unplugged, the active tip of the laser was applied to the ulcer.

Group II – Animals with skin ulcers were subjected to low-level laser irradiation as follows: a semi-conductor diode As–Ga–Al laser at a wavelength of 670 nm (Laser VR-KC-610 Dentoflex, São Paulo, Brazil) was used to deliver a 9 mW treatment that was applied every other day. Power density was estimated as 0.031 W/cm². By administrating 1 J/cm² in four equidistant points on the borders of the circular wound, a total fluence of 4 J/cm² was delivered.

The irradiation time was calculated at 31 s per session (15). To estimate the area at the light beam emission point, a specimeter provided with a scale from 0.1 to 10 mm² was used. The area of the spot size was 28.27×10^{-2} cm². The dose of 4 J/cm² was selected on the basis of previous studies (7).

The animals were euthanized by an overdose of anesthetic. For both experimental groups, tissues representative of the ulcer's borders were removed from all the experimental animals at 3, 7, 10 and 14 days post-surgery and immediately subjected to the following procedures.

Immunohistochemistry

For the demonstration of SM- α actin and desmin, paraffin sections of formalin-fixed tissue were used. Antigen retrieval was accomplished through microwave treatment in citrate buffer at a pH of 6.0. Sections were incubated with the primary antibodies either for anti-SM- α actin (1 : 200) or anti-desmin (1 : 50) (Dako, Carpinteria, CA, USA) overnight at 4 °C in a humidified chamber. Primary antibodies were diluted in 2% BSA in PBS (pH 7.4). After washing in PBS, sections were incubated in 10% skimmed milk during 20 min for blocking non-specific ligations. The slides were then incubated with the secondary antibody: a sheep – anti-Rat IgG conjugated to peroxidase (Dako envision system – labeled polymer Dako) at the dilution of 1 : 1000 for 30 min at 37 °C in a humidified chamber. Blockage of the endogenous peroxidase was performed with 0.3% H₂O₂ for 30 min at room temperature. The color was developed with 0.06% 3,3'-diaminobenzidine tetrahydrochloride (Sigma, St.

Louis, MO, USA) and 0.06% H₂O₂ plus 1% dimethylsulfoxide (Sigma). Sections were counterstained with 1% hematoxylin for 5 min, dehydrated and mounted with Permount. Control sections in which the primary antibody was either omitted or replaced by normal rat serum were used as negative controls. For positive controls, a section of the rat uterus was used.

At the time of sacrifice, fragments of the ulcerated skin were also immediately placed in Tissue-Tek and immersed in liquid nitrogen for a few minutes and kept frozen at – 70 °C in airtight boxes until they were sectioned in a cryostat at – 20 °C. The sections were also subjected to immunohistochemistry for the demonstration of NG2-positive staining cells. The antibody anti-NG2 (Chemicon, Temecula, CA, USA) was used at a dilution of 1 : 100 and followed the same procedure as described above.

Morphometry

For histological analysis, a microscope Motic B5 Professional Series was used with a coupled camera and interlinked to the Motic Image Advance 3.0 computer software. Before using the software, the calibration for each objective was checked by the standard image, captured from a calibration blade provided by the manufacturer. The blades were examined by random selection of three 0.1 mm² areas. The numbers of NG2-, SM- α -actin- or desmin-positive staining cells in the three 0.1 mm² areas were totaled for each animal. Then, each area was captured in the 400 \times increase and saved in a JPEG format.

The morphometric study was performed on the same tissue sections used in the immunohistochemistry analysis. Two blinded examinations were performed by different pathologists. All positive cells were counted, including ones dispersed around blood vessels (pericyte phenotype) and in the ECM (myofibroblast phenotype).

Transmission electron microscopy

Tiny fragments of the skin (about 1 mm³) were immediately fixed by immersion into 4% glutaraldehyde in 0.2 M cacodylate buffer, pH 7.4, for 1 h at 4 °C, washed in buffer and post-fixed with 1% osmium tetroxide, dehydrated in graded concentrations of acetone and embedded in Poly-bed 812 (Embedding Media Polysciences, Warrington, PA, USA, IVC). Selected ultrathin sections (50–70 nm) were made with a Reichert (Ultratome Supernova Leica, Wien, Austria) ultramicrotome and mounted on uncoated copper grids, contrasted with uranyl acetate and a lead citrate. Specimens were examined using a Zeiss EM-9 electron microscope (Oberkochen, Baden-Württemberg, Germany), which was operated at an acceleration voltage of 50 kV.

Statistical analysis

Data were registered in Excel[®] 2007 (Microsoft) and the non-parametric Wilcoxon's Exact test was used to test for differences between the number of NG2-, SM- α -actin- or desmin-positive staining cells measured morphometrically among samples from

laser-treated and untreated wounds. Results were considered significant at $P < 0.05$.

Results

On day 3 post-biopsy, histological changes exhibited a transition from the exudative phase to the proliferative phase of inflammation. Granulation tissue was represented by marked vascular and cellular proliferation, with a predominance of fibroblasts (Fig. 1). The new capillary network exhibited a

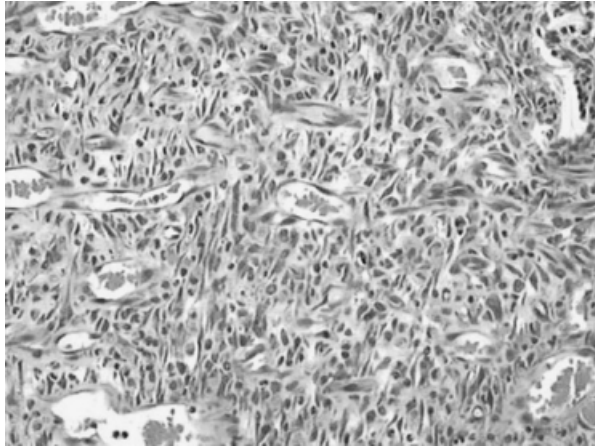


Fig. 1. Granulation tissue characterized by numerous fusiform cells and proliferating capillaries. Laser group, 7 days after the surgical procedure. Hematoxylin–eosin staining.

significant number of desmin- and NG2-positive staining cells in the laser group ($P < 0.05$). They are located around blood vessels and they were identified as pericytes (pericyte phenotype). Both experimental groups also presented several scattered fusiform desmin-, NG2- and SM- α -actin-positive staining cells in the connective tissue. These cells exhibit a so-called ‘myofibroblast phenotype.’ However, there were no significant differences between laser-treated animals and controls at this period of death.

Seven days after the surgical procedure, tissues surrounding laser-treated wounds had significantly more NG2-positive staining cells around proliferating blood vessels than those observed in the untreated control group ($P < 0.05$, Table 1). Positive staining cells for any of the antibody used to appear distributed, especially around newly formed capillaries, which composed the granulation tissue (Figs 2 and 3). The myofibroblast phenotype was more evident for the laser-treated group, as compared with controls (Table 1). Cells expressing anti-NG2, anti-SM- α -actin or anti-desmin were seen around capillaries and arterioles, and also as isolated cells dispersed within the interstitial tissue (Figs 4 and 5). Ultrastructural examination revealed the presence of pericytes appearing as elongated cells within the proliferated capillary basement membrane, with their indented nucleus and cytoplasmic projections (Fig. 6). In addition, many fibroblasts and myofibroblasts appeared to be distributed within the interstitial tissue (Fig. 7).

On day 10, the granulation tissue was observed to exhibit more myofibroblasts, while angiogenesis and pericytes seemed

Table 1. Number of NG2+, desmin+ and SM- α -actin+ cells in control and laser-treated groups, disposed around blood vessels and exhibiting a pericytic or myofibroblastic phenotype

Histological evaluation	Median (interquartile range)			
	Day 3	Day 7	Day 10	Day 14
NG2+ cells (pericytes)†				
Laser treatment	57.0 (55.0–59.0)*	61 (59.0–62.0)*	47.0 (45.0–48.0)	14.0 (6.5–18.0)
Control	33.0 (24.0–42.0)	33 (28.0–35.0)	33.0 (27.0–34.0)	9.0 (0.0–12.0)
NG2+ cells (myofibroblasts)‡				
Laser treatment	11.0 (9.0–11.0)	24.0 (19.0–24.0)*	14.0 (12.0–15.0)	9.0 (3.0–12.0)
Control	10.0 (9.0–11.0)	14.0 (12.0–16.0)	10.0 (4.0–14.0)	0.0 (0.0–5.0)
Desmin+ cells (pericytes)†				
Laser treatment	63.0 (60.0–81.0)*	45.0 (33.0–48.0)	32.0 (30.0–38.0)	20.5 (17.0–29.0)
Control	32.0 (27.0–33.0)	30.0 (29.0–32.0)	33.0 (30.0–33.0)	18.0 (16.0–27.0)
Desmin+ cells (myofibroblasts)‡				
Laser treatment	48.0 (45.0–54.0)	83.0 (82.0–91.0)	65.0 (63.0–75.0)	31.0 (28.0–37.5)
Control	45.0 (40.0–53.0)	62.0 (54.0–63.0)	47.0 (33.0–54.0)	30.0 (20.0–33.0)
SM- α -actin+ cells (pericytes)†				
Laser treatment	88.0 (73.0–93.0)	45.0 (43.0–50.0)	54.0 (48.0–66.0)*	33.0 (32.50–34.50)
Control	77.0 (54.0–81.0)	44.0 (38.0–55.0)	28.0 (25.0–43.0)	38.0 (33.0–41.0)
SM- α -actin+ cells (myofibroblasts)‡				
Laser treatment	24.0 (23.0–28.0)	85.0 (69.0–92.0)*	54.0 (50.0–75.0)	34.0 (32.0–36.0)
Control	20.0 (18.0–26.0)	27.0 (24.0–32.0)	57.0 (47.0–81.0)	30.0 (28.0–32.0)

* $P < 0.05$ for comparison between laser treatment and control groups.

†Pericyte phenotype defined as positive cells around blood vessels.

‡Myofibroblast phenotype defined as positive cells in ECM.

ECM, extracellular matrix; SM- α -actin, smooth muscle alpha-actin.

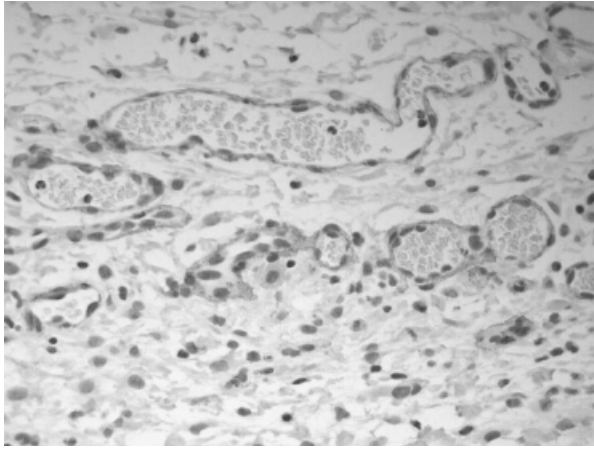


Fig. 2. Smooth muscle α -actin-positive cells disposed around the endothelium. Control group, 3 days after surgery. Immunohistochemistry, anti-smooth muscle α -actin.

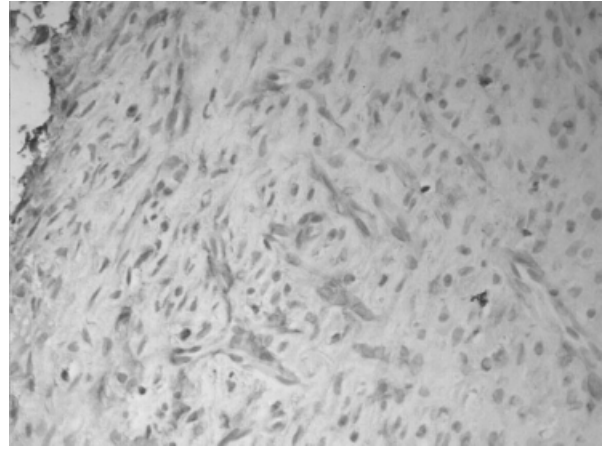


Fig. 4. NG2-positive cells dispersed within the interstitial tissue of a control group animal, seventh day. Immunohistochemistry, anti-NG2.

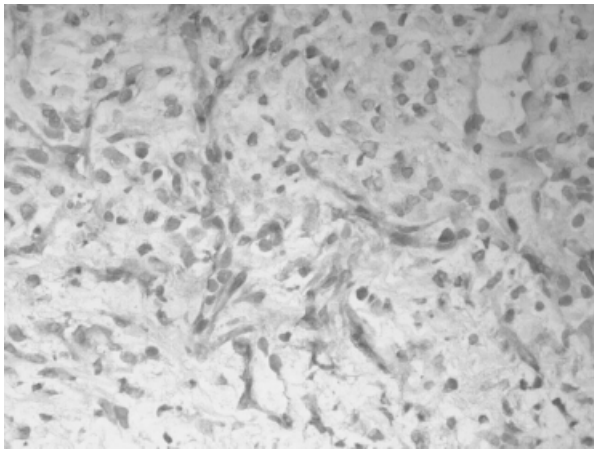


Fig. 3. NG2 positive cells were seen near proliferating capillaries in the granulation tissue. Laser group, third day. Immunohistochemistry, anti-NG2.

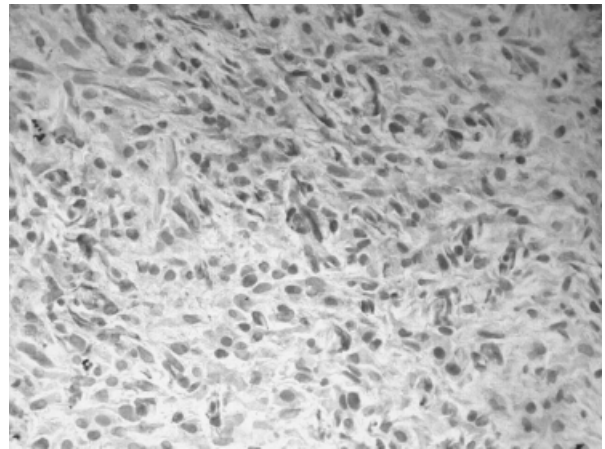


Fig. 5. Desmin-positive cells were found isolated in the granulation tissue of a laser group, seventh day. Immunohistochemistry, anti-desmin.

to be less apparent. Statistical significance was observed for marked anti-SM- α -actin cells (Table 1). Numerous SM- α -actin-positive staining cells were observed close to the endothelium, without any peculiar pattern of distribution in the laser-treated group. Those marked for anti-NG2 were predominantly found to be integrated to muscular media of the small arterioles. These cells were dispersed in the ECM and appeared as isolated entities, exhibiting phenotypic modulation toward myofibroblasts.

Around the 14th experimental day, some anti-NG2-, anti-desmin- and anti-SM- α -actin-positive staining cells were seen in the dermis, but no statistical differences were observed among the analyzed samples (Table 1).

Discussion

The results of the present study demonstrate that 670 nm LLLT increased the number of SM- α -actin-, desmin- and NG2-positive

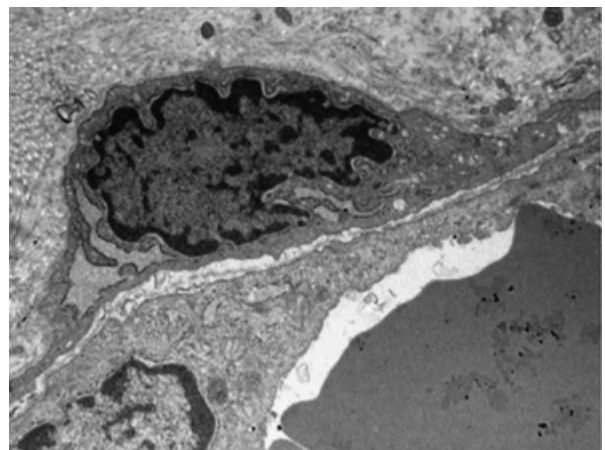


Fig. 6. A pericyte lying on the basal membrane and adjacent to the endothelial cell from a laser group animal, seventh day. Electron micrograph.

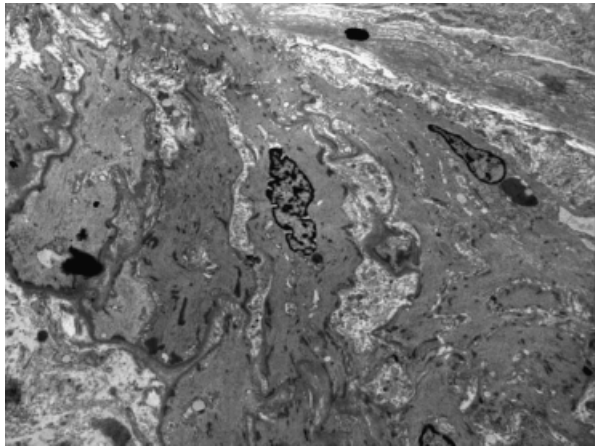


Fig. 7. A group of myofibroblasts exhibiting indented nucleus (arrows) and an electron-dense material along the cytoplasmic membrane. Laser group animal, seventh day. Electron micrograph.

staining cells during the initial period of tissue repair. Laser therapy contributed to the recruitment of pericytes located around the endothelium. Pericytes have the ability to differentiate into several cell types, including myofibroblasts, to bring about tissue contraction, which is essential for tensile strength of the wounded tissue (12).

The intense fibroblastic and myofibroblastic proliferation present in the granulation tissue, which is related to wound contraction, used to be considered deriving from resident fibroblasts or undifferentiated mesenchymal cells. However, it has been suggested that pericytes are the main source (16). Although there are no specific antibodies for pericytes, SM- α -actin, desmin and, more recently, NG2 can help their identification (17). The present study confirmed the presence of all of these molecules. The perivascular location of pericytes and the interstitial situation of myofibroblasts also aid positive identification of these cells. SM- α -actin-positive staining cells were seen throughout the interstitial matrix in laser-treated animals, but were more commonly observed near proliferating blood vessels. The same finding *in vivo* was described by studying tissue sections obtained from extraction of third molars irradiated with low-level laser (18).

Pericytes are receiving considerable attention nowadays. The role of pericytes in vascular stability in newly formed blood vessels has been stressed (10). With their long cytoplasmic prolongations that extend the endothelial tube, they establish focal contacts with the endothelium through specialized junctions. Furthermore, pericytes can activate signals and deposit ECM that may influence endothelium stability and quiescence. A failure of the neural adhesion molecule in neoplastic pancreas β -cells has been demonstrated to result in fragile blood vessels due to a disturbance between endothelial cells and pericytes, with the deposition of an abnormal perivascular matrix (11). The authors suggested that such vascular instability facilitated metastasis, stressing the importance of pericyte–endothelium interaction. Pericytes can also release angiopoietin-1 (19). This molecule is attached to

endothelial cells receptors, stabilizing the interaction of these cells with the other mural cells. Under stress conditions the endothelial cells synthesize angiopoietin-2, which blocks the interaction of angiopoietin-1 with its receptor, facilitating the migration of endothelial cells to where the formation of new blood vessels would be expected. In our ultrastructural findings, pericytes were observed to be in close association with endothelium, sharing its basal membrane. Their typical localization was the main parameter to identify them.

Some authors have described LLLT as an additional modality of therapy capable of modulating the ECM elements, both quantitatively and qualitatively (20–22). For instance, the distribution and orientation of collagen fibers is more organized in experimental groups treated with laser (23, 24). Other authors described an increase in local circulation after laser irradiation (25, 26). However, the elevation of local temperature after irradiation was not taken into consideration because LLLT, as opposed to high-power lasers, causes no significant changes in tissue temperature. The newly formed vasculature allows for fluid, oxygen, nutrients and immunocompetent-cells exchange (27). Previous studies from our group, as well as from others, already demonstrated an increase in vascular density following LLLT. This finding has been described to a laser-induced higher oxygen tension within the damaged tissue. Angiogenesis is an important structural component of tissue repair because it always precedes collagen synthesis and deposition.

Therefore, how do pericytes and myofibroblasts participate in tissue repair? The statistically significant increase in the number of pericytes and myofibroblasts observed in the laser-treated group 3–7 days following the skin injury strongly suggests laser influence on cellular phenotypic modulation. The identical immunohistochemical pattern exhibited by both pericytes and myofibroblasts suggests a common origin of these cells, the newly transformed myofibroblasts then contributing to wound contraction. Thus, vascular proliferation, besides securing oxygen supply to the newly formed repair tissue, also secures a new cellular population, represented by pericytes, capable of proliferation and differentiation along the repair process.

Other studies using molecular approaches are necessary in order to verify the source of pericytes and how LLLT and these cell interactions are processed during tissue repair.

References

1. Karu T. Photobiology of low-power laser effects. *Health Phy* 1989; **56**: 691–704.
2. Passarella S, Casamassima E, Molinari S, et al. Increase of proton electrochemical potential and ATP synthesis in rat liver mitochondria irradiated *in vitro* by helium-neon laser. *FEBS Lett* 1984; **175**: 95–99.
3. Pereira ANP, Eduardo CP, Matson E, Marques MM. Effect of low-power laser irradiation on cell growth and procollagen synthesis of cultured fibroblasts. *Lasers Surg Med* 2002; **31**: 263–267.
4. Pugliese LS, Medrado ARAP, Reis SRA, Andrade ZA. The influence of low-level laser therapy on biomodulation of collagen and elastic fibers. *Pesqui Odontol Bras* 2003; **17**: 307–313.

5. Vinck EM, Cagnie BJ. Increased fibroblast proliferation induced by light emitting diode and low power laser irradiation. *Lasers Med Sci* 2003; **18**: 95–99.
6. Carrinho PM, Renno AC, Koeke P, Salate AC, Parizotto NA, Vidal BC. Comparative study using 685-nm and 830-nm lasers in the tissue repair of tenotomized tendons in the mouse. *Photomed Laser Surg* 2006; **24**: 754–758.
7. Medrado ARAP, Pugliese LS, Reis SRA, Andrade ZA. Influence of low level laser therapy on wound healing and its biological action upon myofibroblasts. *Lasers Surg Med* 2003; **32**: 239–244.
8. Schlingemann RO, Rietveld FJR, Kwaspen F, Van de Kerkhof PCM, Waal RMW, Ruiter DJ. Differential expression of markers for endothelial cells, pericytes, and basal lamina in the microvasculature of tumors and granulation tissue. *Am J Pathol* 1991; **138**: 1335–1347.
9. Von Tell D, Armulik A, Betsholtz C. Pericytes and vascular stability. *Exp Cell Res* 2006; **312**: 623–629.
10. Allt G, Lawrenson JG. Pericytes: cell biology and pathology. *Cells Tissues Organs* 2001; **169**: 1–11.
11. Xian X, Hakansson J, Stahlberg A, et al. Pericytes limit tumor cell metastasis. *J Clin Invest* 2006; **116**: 642–651.
12. Farrington-Rock C, Crofts NJ, Doherty MJ, et al. Chondrogenic and adipogenic potential of microvascular pericytes. *Circulation* 2004; **110**: 2226–2232.
13. Ponti G, Peretto P, Bonfanti L. Genesis of neuronal and glial progenitors in the cerebellar cortex of peripuberal and adult rabbits. *PLoS One* 2008; **3**: e2366.
14. Rajkumar VS, Howell K, Csiszar K, Denton CP, Black CM, Abraham DJ. Shared expression of phenotypic markers in systemic sclerosis indicates a convergence of pericytes and fibroblasts to a myofibroblast lineage in fibrosis. *Arthritis Res Ther* 2005; **7**: 1113–1123.
15. Tunér J, Hode L. *Laser therapy in dentistry and medicine*. Spjutvägen: Prima Books, 1996.
16. Eyden B. The myofibroblast: a study of normal, reactive and neoplastic tissues, with emphasis on ultrastructure. Part 1 – normal and reactive cells. *J Submicrosc Cytol Pathol* 2005; **37**: 109–204.
17. Barberi T, Klivenyi P, Calingasan NY, et al. Neural subtype specification of fertilization and nuclear transfer embryonic stem cells and application in parkinsonian mice. *Nat Biotechnol* 2003; **21**: 1200–1207.
18. Pourreau-Schneider N, Ahmed A, Soudry M, et al. Helium-neon laser treatment transforms fibroblasts into myofibroblasts. *Am J Pathol* 1990; **137**: 171–178.
19. Takakura N. Role of hematopoietic lineage cells as accessory components in blood vessel formation. *Cancer Sci* 2006; **97**: 568–574.
20. Enwemeka CS, Parker JC, Dowdy DS, Harkness EE, Sanford LE, Woodruff LD. The efficacy of low-power lasers in tissue repair and pain control: a meta-analysis study. *Photomed Laser Surg* 2004; **22**: 323–329.
21. Fung DTC, Ng GYF, Leung MCP, Tay DKC. Effects of a therapeutic laser on the ultrastructural morphology of repairing medial collateral ligament in a rat model. *Lasers Surg Med* 2003; **32**: 286–293.
22. Nascimento PM, Pinheiro AL, Salgado MAC, Ramalho L. A preliminary report on the effect of the healing of cutaneous surgical wounds as a consequence of an inversely proportional relationship between wavelength and intensity: histological study in rats. *Photomed Laser Surg* 2004; **22**: 513–518.
23. Garavello-Freitas I, Baranauskas V, Joazeiro PP, Padovani CR, Pais-Silva MD, Cruz-Höfling MA. Low-power laser irradiation improves histomorphometrical parameters and bone matrix organization during tibia wound healing in rats. *J Photochem Photobiol* 2003; **70**: 81–89.
24. Reis SRA, Medrado ARAP, Marchionni AMT, Figueira C, Fracassi LD, Knop LAH. Effect of 670-nm laser therapy and dexamethasone on tissue repair: a histological and ultrastructural study. *Photomed Laser Surg* 2008; **26**: 307–313.
25. Medrado ARAP, Trindade E, Reis SRA, Andrade ZA. Action of low-level laser therapy on living fatty tissue of rats. *Lasers Med Sci* 2006; **21**: 19–23.
26. Schindl A, Schindl M, Schindl L, Jurecka W, Hönigsmann H, Breier F. Increased dermal angiogenesis after low-intensity laser therapy for a chronic radiation ulcer determined by a video measuring system. *J Am Acad Dermatol* 1999; **40**: 481–484.
27. Ponce AM, Price RJ. Angiogenic stimulus determines the positioning of pericytes within capillary sprouts in vivo. *Microvasc Res* 2003; **65**: 45–48.